

## ANGULAR CLUSTERING OF X-RAY POINT-LIKE SOURCES IN THE XMM LARGE SCALE STRUCTURE SURVEY

O. Garcet<sup>1</sup>, P. Gandhi<sup>2</sup>, E. Gosset<sup>1</sup>, A. Gueguen<sup>3</sup>, F. Pacaud<sup>3</sup>, M. Pierre<sup>3</sup>, and J. Surdej<sup>1</sup>

<sup>1</sup>Institut d'Astrophysique et de Géophysique, Université de Liège, Belgium

<sup>2</sup>European Southern Observatory, Casilla 19001, Santiago, Chile

<sup>3</sup>CEA/DSM/DAPNIA Service d'Astrophysique, Saclay, F-91191 Gif sur Yvette, France

### ABSTRACT

We present the log(N)-log(S) diagram and an angular clustering analysis of point-like X-ray sources for the XMM-Newton Large Scale Structure (XMM-LSS) Survey. Though designed to study the properties and evolution of distant X-ray clusters up to  $z \sim 1$ , the large contiguous area planned for the full XMM-LSS survey is ideal for studying X-ray-selected AGN and their clustering properties. Our goal is to test the AGN unified scheme paradigm by studying the clustering of X-ray point-like sources. A clustering analysis of a  $4.2 \text{ deg}^2$  contiguous region in the soft ([0.5-2] keV) and hard ([2-10] keV) energy bands is presented here. The angular correlation function and the nearest neighbour test have been performed in each band. Both tests only reveal a weak clustering in the soft X-ray band.

### 1. THE XMM-LSS SURVEY

The XMM-LSS observations consist presently of 51 overlapping pointings with exposure time between 10 and 20 ks, which cover a total contiguous area of  $6 \text{ deg}^2$ . Full details of the detection pipeline and source classification will be presented in Pacaud et al. (2005).

### 2. SELECTION OF POINT-LIKE SOURCES

Only those sources that lie within 10 arcmin of the optical axis centres of each pointing were retained. This was done in order to minimize biases due to the PSF distortion at large off-axis angles. Confirmed extended X-ray sources were removed from the [0.5-2] keV (soft) sample, while for the [2-10] keV (hard) sample, every source was considered as point-like. Finally, all samples in this analysis have been defined with  $S/N > 3$ .

### 3. GENERATION OF RANDOM (UNCORRELATED) CATALOGUES

Significant variation in sensitivity and irregular holes are present in our survey. That is why it has been crucial to simulate selection effects accurately. Due to mirror vignetting, the minimum detectable flux at an off-axis distance of 10 arcmin is higher by a factor of 2 as compared to the optical-axis centre. We generated an ensemble of random and initially uniform catalogues to correctly simulate the selection effects of the sample, each catalogue containing the same number of sources as the parent data sample. These random catalogues have been generated in the following way : first, sky positions over the central inner 10 arcmin regions of each pointing are randomly chosen. Second, source flux are randomly chosen, according to the logN-logS of the parent data sample. Finally, the source flux at a given position is compared to the limiting flux at that location. If the limiting flux at that position is higher, the random source is discarded and another sky position is again randomly chosen.

### 4. RESULTS

Results concerning the logN-logS are shown in Fig 1. and Fig 2. for the soft and hard band, respectively. We systematically find significantly less bright sources (only shown for the hard band, compared to the HEL-LAS2XMM). Clustering analysis results are gathered in Fig 3. to Fig 6. Both tests (ACF and nearest neighbour test) only reveal a weak clustering in the soft band, and no hint for clustering in the hard band.

### 5. DISCUSSION AND CONCLUSION

We presented a clustering analysis over a region covering  $4.2 \text{ deg}^2$  in the soft and hard energy bands. In the soft band, both the two-point angular correlation function and

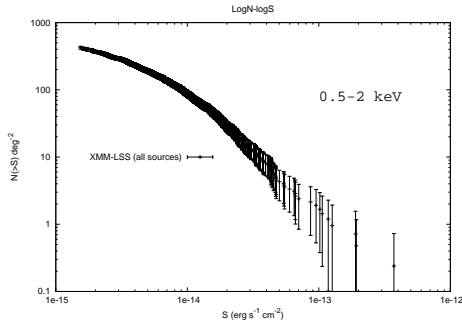


Figure 1. LogN-logS for the soft sample, in the [0.5-2] keV band. The logN-logS is shown here for all sources (clusters have a minor contribution, except at very bright fluxes). The error bars denote  $1\sigma$  Poisson uncertainties.

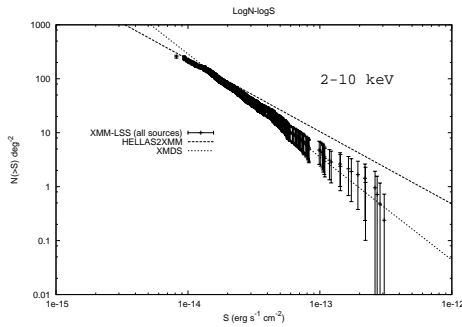


Figure 2. LogN-logS for the hard sample, in the [2-10] keV band. The logN-logS is shown here for all sources. The error bars denote  $1\sigma$  Poisson uncertainties.

the nearest neighbour test show a positive clustering signal, though with low significance, around  $2\sigma$ , which is consistent with measurements of Basilakos (2005) within the error bars. However, the results of the same analysis in the hard band is consistent with a random and uniform distribution, which is at odds with measurements of Basilakos (2004). Full details of this clustering analysis are presented in Gandhi et al. (2005).

## REFERENCES

- Baldi A., Molendi S., Comastri A., et al. 2002, ApJ, **564**, 190
- Basilakos S., Georgakakis A., Plionis M., et al. 2004, ApJL, **607**, L79
- Basilakos S., Plionis M., Georgakakis A., et al. 2005, MNRAS, **356**, 183
- Chiappetti L., Tajer M., Trinchieri G., et al. 2005, A&A, **439**, 413
- Gandhi P., Garcet O., Disseau L., et al., submitted to MNRAS
- Hamilton A. J. S., 1993, ApJ, **417**, 19
- Pacaud F., Pierre M., Gueguen A., et al. 2005, to be submitted to MNRAS

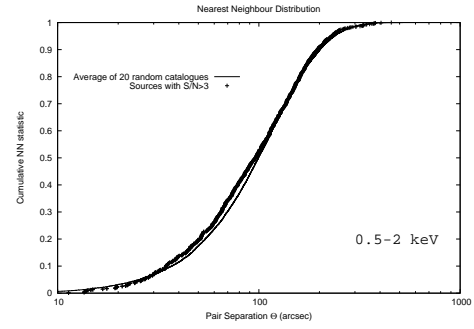


Figure 3. Cumulative first nearest-neighbour distribution function in the [0.5-2] keV band, for point-like sources, compared to the average distribution function of random catalogues.

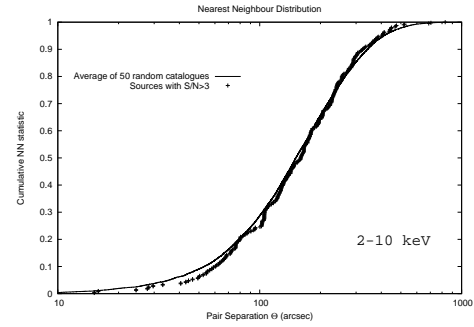


Figure 4. Cumulative first nearest-neighbour distribution function in the [2-10] keV band, for point-like sources, compared to the average distribution function of random catalogues.

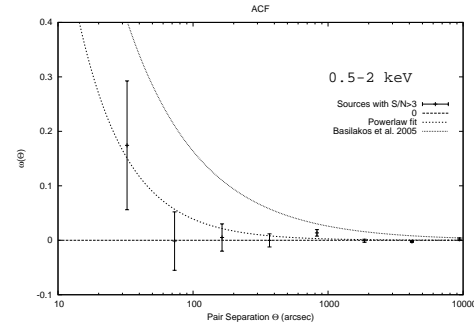


Figure 5. ACF, as defined by Hamilton (1993) and measured for the soft (1163 sources) point-sources. The dashed line is the best-fit powerlaw model. Literature determination of the best-fit powerlaw ACF from Basilakos (2005) is shown.

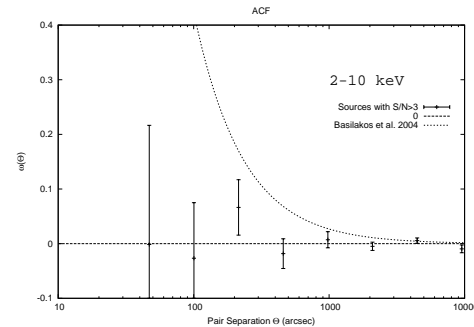


Figure 6. ACF, as defined by Hamilton (1993) and measured for the hard (413 sources) point-sources. Literature determination of the best-fit powerlaw ACF from Basilakos (2004) is shown.